FP-APW+lo calculations of the electronic and optical properties of alkali metal sulfides under pressure

2009 J. Phys.: Condens. Matter 21 095404

(http://iopscience.iop.org/0953-8984/21/9/095404)

J. Phys.: Condens. Matter **21** (2009) 095404 (9pp) doi:10.1088/0953-8984/21/9/095404

FP-APW + lo calculations of the electronic and optical properties of alkali metal sulfides under pressure

H Khachai[1], R Khenata[2,6], A Bouhemadou[3,6], A Haddou[1], Ali H Reshak[4,5], B Amrani[2], D Rached[1] and B Soudini[1]

[1] Applied Materials Laboratory (AML), Electronics Department, University of Sidi-bel-Abbes, Sidi-bel-Abbes 22000, Algeria
[2] Laboratoire de Physique Quantique et de Modélisation Mathématique (LPQ3M), Département de Technologie, Université de Mascara, Mascara 29000, Algeria
[3] Laboratory for Developing New Materials and their Characterization, Department of Physics, Faculty of Science, University of Setif, Setif 19000, Algeria
[4] Institute of Physical Biology, South Bohemia University, Nove Hrady 373 33, Czech Republic
[5] Institute of System Biology and Ecology, Academy of Sciences, Nove Hrady 373 33, Czech Republic

E-mail: khenata_rabah@yahoo.fr and a_bouhemadou@yahoo.fr

Received 21 October 2008
Published 30 January 2009
Online at stacks.iop.org/JPhysCM/21/095404

Abstract

The electronic and optical properties of M_2S (M = Li, Na, K and Rb) compounds in the cubic antifluorite structure have been calculated, using a full relativistic version of the full-potential augmented plane-wave plus local orbitals method based on density functional theory, within both the local density approximation (LDA) and the generalized gradient approximation (GGA). Moreover, the Engel–Vosko GGA formalism (EV-GGA) is applied so as to optimize the corresponding potential for band structure calculations. The calculated equilibrium lattices and bulk moduli are in good agreement with the available data. Band structure, density of states, electron charge density and pressure coefficients of energy gaps are given. Results obtained for band structure using EV-GGA are larger than those with LDA and GGA. It is found that the spin–orbit coupling lifts the triple degeneracy at the Γ point and the double degeneracy at the X point. The analysis of the electron charge density shows that the M–S bonds have a significant ionic character. The complex dielectric functions $\varepsilon_2(\omega)$ for alkali metal sulfides were calculated for radiation up to 30 eV and the assignment of the critical points to the band structure energy differences at various points of the Brillouin zone was made. The pressure and volume dependence of the static dielectric constant and the refractive index are calculated.

(Some figures in this article are in colour only in the electronic version)

1. Introduction

There is a growing interest in the study of materials with chemical formula AB_2 crystallizing in the fluorite and antifluorite structures, due to their technological importance in the field of solid-state ionics. Among this family of materials, the alkali metal sulfides, Li_2S, Na_2S, K_2S and Rb_2S, crystallize at ambient conditions in the cubic antifluorite structure (anti-CaF_2 type) (No 225) [1]. The sulfur atoms are located at (0; 0; 0) and the metal atoms are located at (0.25; 0.25; 0.25) positions. These compounds are characterized by their large bandgaps and their high ionic conductivity. The high ionic conductivity in these compounds arises as a consequence of Frenkel-defect formation by metal atoms redistributing on their regular sites as well as on the interstitial sites without

[6] Authors to whom any correspondence should be addressed.

any significant distortion of the FCC sulfur sublattice. This is so mainly because of the less compact crystal structure of antifluorite-type structure in comparison to that of fluorite-type structure.

The alkali metal sulfides M_2S (M = Li, Na, K and Rb) appear to be promising candidates for several technological applications. They find applications in solid-state batteries [2–4].They are used as high capacity energy storage devices for electric vehicles [5] and as a power source for portable electronic devices such as mobile phones, video cameras and notebook-type personal computers [6].

Only a few experimental works have been devoted to exploring the physical properties of these compounds; they focused on the elastic properties [7, 8] and the structural phase transformation [9–11]. Theoretically, Lichanot *et al* [12] and Buhrer and co-workers [13] investigated the structural and elastic properties of Li_2S and Na_2S compounds, using the linear combination of atomic orbitals method (LCAO) and the shell model, respectively. Schön *et al* [14] performed the Hartree–Fock linear combination of atomic orbitals method (LCAO-HF) for the high pressure structural phase transition of these compounds. The electronic band structure of these materials at ambient conditions has been discussed by Zhuravlev *et al* [15], Azavant *et al* [16] and Eithiraj *et al* [17], using the self-consistent pseudopotential method (PP), the LCAO-HF and the tight-binding linear muffin-tin orbital method (TB-LMTO), respectively.

To the best of our knowledge, there are no earlier theoretical calculations for the optical properties and bandgap pressure dependences for these compounds. The knowledge of the electronic and optical properties of materials under the effect of pressure provides insight about their performance in practical applications. It is therefore timely to investigate these properties for Li_2S, Na_2S, Ki_2S and Rb_2S compounds in order to provide another reference for the existing theoretical work on this fascinating class of materials, using the full-potential augmented plane-wave plus local orbitals method (FP-APW + lo) within the density functional theory (DFT), which has proven to be one of the most accurate methods for the computation of the electronic structure of solids [18, 19].

2. Computational method

The calculations reported here were carried out using a full relativistic version of the full potential with the mixed basis APW + lo method [20, 21] as implemented in the WIEN2K computer package [22]. In this method the space is divided into an interstitial region (IR) and non-overlapping muffin-tin (MT) spheres centered at the atomic sites. In the IR region, the basis set consists of plane waves. Inside the MT spheres, the basis set is described by radial solutions of the one particle Schrödinger equation (at fixed energy) and their energy derivatives multiplied by spherical harmonics. The exchange–correlation effects for the structural properties are treated by the local density approximation (LDA) [23] with and without the generalized gradient approximation (GGA) [24]. Moreover, the alternative form of GGA proposed by Engel and Vosko (EV-GGA) [25] is also used for the band structure calculations.

In order to achieve energy eigenvalue convergence, the wavefunctions in the interstitial region were expanded in plane waves with a cut-off $K_{max} = 12/R_{MT}$, where R_{MT} denotes the smallest atomic sphere radius and K_{max} gives the magnitude of the largest K vector in the plane-wave expansion. The R_{MT} are taken to be 1.5, 2.2, 2.1, 2.8 and 3.0 atomic units (a.u.) for Li, S, Na, K and Rb, respectively. The valence wavefunctions inside the spheres are expanded up to $l_{max} = 9$, while the charge density was Fourier expanded up to $G_{max} = 12$ (a.u.). The self-consistent calculations are considered to be converged when the total energy of the system is stable within 10^{-4} Ryd. The integrals over the Brillouin zone are performed up to 18 k-points in the irreducible Brillouin zone, using the Monkhorst–Pack special k-point approach [26].

3. Results and discussion

3.1. Structural properties

In order to calculate the ground-state properties of the alkali metal sulfides, Li_2S, Na_2S, K_2S and Rb_2S, the total energies are calculated at different volumes ranging from 1.2 to $0.6V_0$, where V_0 is the unit cell equilibrium volume. The calculated total energies are fitted to the Birch equation of state [27] to determine the ground-state properties such as the equilibrium lattice parameter a_0, the bulk modulus B_0, and the pressure derivative of the bulk modulus B'. The calculated a_0, B_0 and B' for Li_2S, Na_2S, K_2S and Rb_2S are given in table 1 together with the available experimental and theoretical data. They are in good agreement with the experimental ones [8, 28]. The computed lattice constant a using LDA and GGA deviates from the measured ones within 2.4 and 0.05%, respectively, in Li_2S; 2.2 and 0.9%, respectively, in Na_2S; 2.6 and 1.1%, respectively, in K_2S and 1.6 and 2.0%, respectively, in Rb_2S. This ensures the reliability of the present first-principles computations. We note that the use of the LDA slightly underestimates the lattice constants and slightly overestimates the bulk modulus compared to the experimental values, while the GGA slightly overestimates the lattice constants and slightly underestimates the bulk modulus compared to the measurements. The calculated bulk modulus decreases when we move from Li_2S to Na_2S to K_2S to Rb_2S.

3.2. Electronic properties

The self-consistent full relativistic band structures of Li_2S, Na_2S, K_2S and Rb_2S were obtained in the cubic antifluorite phase at equilibrium volume within LDA, GGA and EV-GGA schemes.

It is well known that the LDA and GGA usually underestimate the energy gap [29, 30]. This is mainly due to the fact that they have simple forms that are not sufficiently flexible to accurately reproduce both exchange–correlation energy and its charge derivative. Engel and Vosko, by considering this shortcoming, constructed a new functional form of the GGA which has been designed to give better exchange potential at the expense of less agreement as regards exchange energy. This approach, which is called the EV-GGA, yields a better band splitting and some other properties which

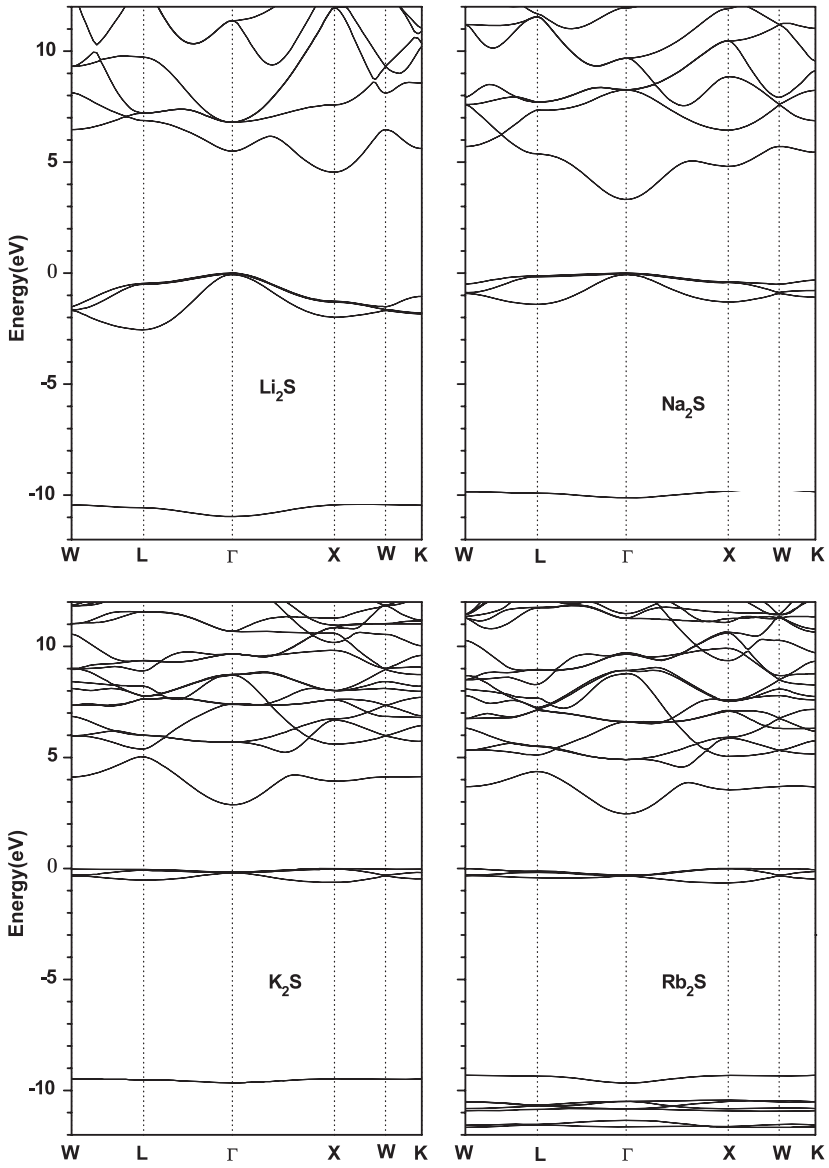

Figure 1. Calculated band structure for Li_2S, Na_2S, K_2S and Rb_2S compounds within EV-GGA.

mainly depend on the accuracy of the exchange–correlation potential [31, 32]. On the other hand, in this method, the quantities which depend on an accurate description of the exchange energy such as equilibrium volumes and the bulk modulus are in poor agreement with experiment [33]. The calculated band structure profiles using the LDA, GGA and EV-GGA for the compounds studied herein were similar except for the values of their bandgaps which were higher within EV-GGA. Figure 1 shows the calculated band structures at equilibrium volumes for Li_2S, Na_2S, K_2S and Rb_2S within EV-GGA. The overall band profiles are in fairly good agreement with previous theoretical results [15, 17]. The valence band maximum (VBM) is located at the Γ point in Li_2S and Na_2S and at the X point in K_2S and Rb_2S. The conduction band minimum (CBM) occurs at the X point in Li_2S and at the Γ point in Na_2S, K_2S and Rb_2S, resulting in a direct bandgap for Na_2S (Γ–Γ) and an indirect bandgap for Li_2S (Γ–X), K_2S (X–Γ) and Rb_2S (X–Γ) compounds. The calculated bandgaps and valence bandwidths for these compounds are given in table 2, along with the available theoretical results. In view of table 2, it is clear that the calculated bandgaps with EV-GGA are larger than those with LDA and GGA. Figure 2 shows that the spin–orbit interaction lifts the triple degeneracy at the Γ point and the double degeneracy at the X point. The spin–orbit splitting in these compounds is about 0.07 eV and 0.03 eV at the Γ and X points, respectively.

To further elucidate the nature of the electronic band structure, we have also calculated the total and atomic site projected densities of states (PDOS) of these compounds. These are displayed in figure 3. Our results are consistent with those obtained by Eithiraj *et al* [17]. From the PDOS we are able to identify the angular momentum character of the different structures. The first structure located at about −10.7 eV (−10 eV) below the Fermi level for Li_2S (Na_2S) arises mainly from the S 's'-like states. The lowest lying band situated at about −9.6 eV for K_2S and −9.4 eV for Rb_2S is

Table 1. Calculated lattice parameter a_0, bulk modulus B_0 and its pressure derivative B' for Li_2S, Na_2S, K_2S and Rb_2S compounds, along with the experimental and previous theoretical calculations.

	a_0 (Å)	B_0 (GPa)	B'
Li_2S			
Present work: LDA (GGA)	5.569 (5.711)	46.19 (40.40)	3.90 (3.88)
Experiment	5.708[a]	45.7[b]	
Other calculations	5.645[c]	43.45[c]	
	5.811[d]	41.00[d]	
	5.817[e], 5.475[e]	52.46[e], 51.47[e]	
	5.513[e], 5.575[e]	47.55[e], 41.36[e]	
Na_2S			
Present work: LDA (GGA)	6.384 (6.577)	33.63 (27.84)	4.33(4.26)
Experiment	6.526[a]	49.00[b]	
Other calculations	6.428[c]	32.95[c]	
	6.634[d]	28.2[d]	
	6.644[e], 6.264[e]	39.00[e], 38.80[e]	
	6.299[e], 6.375[e]	34.84[e], 29.94[e]	
K_2S			
Present work: LDA (GGA)	7.193 (7.475)	23.70 (19.03)	4.33(4.14)
Experiment	7.391[a]	—	
Other calculations	7.387[c]	27.29[c]	
	7.626[e], 6.981[e]	29.41[e], 28.67[e]	
	7.066[e], 7.779[e]	26.09[e], 21.48[e]	
Rb_2S			
Present work: LDA (GGA)	7.527 (7.806)	21.01 (18.30)	4.47(4.01)
Experiment	7.65[a]	—	
Other calculations	7.599[c]	18.01[c]	
	8.249[e], 7.624[e]	15.04[e], 25.76[e]	
	7.723[e], 6.649[e]	24.26[e], 21.45[e]	

[a] Reference [28]; [b] reference [8]; [c] reference [17]; [d] reference [16]; [e] reference [14].

due mainly to the S 's'-like states. The upper valence band (UVB) that lies close to the Fermi level is dominated by the 'p'-like states of the S atoms. The conduction band is complex in nature, which arises due to the hybridization of anion and cation states. The bottom of the conduction band in Li_2S is a mixture of S 's, p and d' and Li 's and p'-like states. In Na_2S, K_2S and Rb_2S, the bottom of the conduction is made up predominantly 'p'-like states of S atoms and 'd'-like states of the metal atoms with a contribution from 's and d'-like states of S atoms and 's and p'-like states of metal atoms. The bottom of the conduction band for Na_2S, K_2S and Rb_2S is separated from the rest by an energy gap.

The present calculated upper valence band bandwidth (UVBW) is larger than that obtained by using the TB-LMTO [15] and pseudopotential [17] calculations. We note that the UVBW decreases as the size of metal ion M (M = Li, Na, K, Rb) increases. This is because as the size of the metal ion increases the interatomic S–S distance increases in going from Li_2S to Na_2S to K_2S to Rb_2S, leading to reduced overlap between the neighboring states.

To predict the bonding nature of solids, the electronic density calculation within the framework of the first principle approach can be used [34, 35]. In figure 4, we show the total valence charge densities in the (110) plane for each material. The numbers labelling the contours in this figure are in units

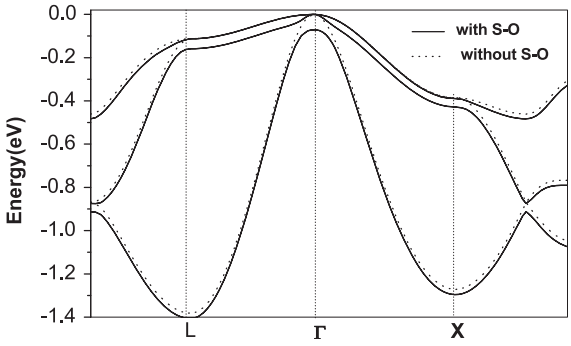

Figure 2. EV-GGA band structure of Na_2S with and without SO coupling for energies close to the Fermi level.

Table 2. Energy bandgaps (in eV) and upper valence bandwidth UVBW (in eV) for Li_2S, Na_2S, K_2S and Rb_2S compounds in the cubic antifluorite phase.

	Present work			Other calculations	
	EV-GGA	GGA	LDA	TB-LMTO[a]	Pseudopotential[b]
Li_2S					
Γ–Γ	5.50	4.19	3.97	4.456	4.46
Γ–X	4.55	3.36	3.14	3.297	3.15
X–X	5.81	4.77	4.59		
UVBW	2.54	2.87	2.93	1.822	1.91
Na_2S					
Γ–Γ	3.32	2.40	2.16	2.566	3.05
Γ–X	3.70	2.85	2.64	3.037	
X–X	5.20	4.27	4.08		
UVBW	1.47	1.63	1.97	0.620	1.17
K_2S					
Γ–Γ	3.02	2.40	2.19	2.683	3.15
X–Γ	2.86	2.24	2.01	2.464	3.11
X–X	3.93	3.41	3.26		
UVBW	0.63	0.65	0.68	1.219	0.38
Rb_2S					
Γ–Γ	2.76	2.28	2.08	2.795	3.15
X–Γ	2.46	1.94	1.68	2.348	2.97
X–X	3.77	3.11	2.82		
UVBW	0.63	0.66	0.78	0.215	0.42

[a] Reference [17]; [b] reference [15].

of electrons per cubic angstrom. Visual comparison of the corresponding charge density plots indicates that the bonding nature of these compounds is mainly ionic, which explains their insulation behavior.

In figure 5, we show the pressure dependence of the UVBW for Li_2S, Na_2S, K_2S and Rb_2S compounds. The UVBW increases with increasing pressure from 0 to 12 GPa; such behavior is consistent with previous calculations on binary compounds [36].

In order to investigate the effect of the pressure on the size of the energy gaps of these compounds in the antifluorite structure, we have calculated at different sets of pressures the direct and indirect bandgaps. Figure 6 shows the plots of the pressure variation of the main direct and indirect bandgaps of M_2S compounds within the EV-GGA approximation. The bandgap pressure data are well fitted to a quadratic function: $E_g(P) = E_g(0) + BP + CP^2$, where E_g is in eV, the pressure P is in GPa, and B and C are the linear and quadratic

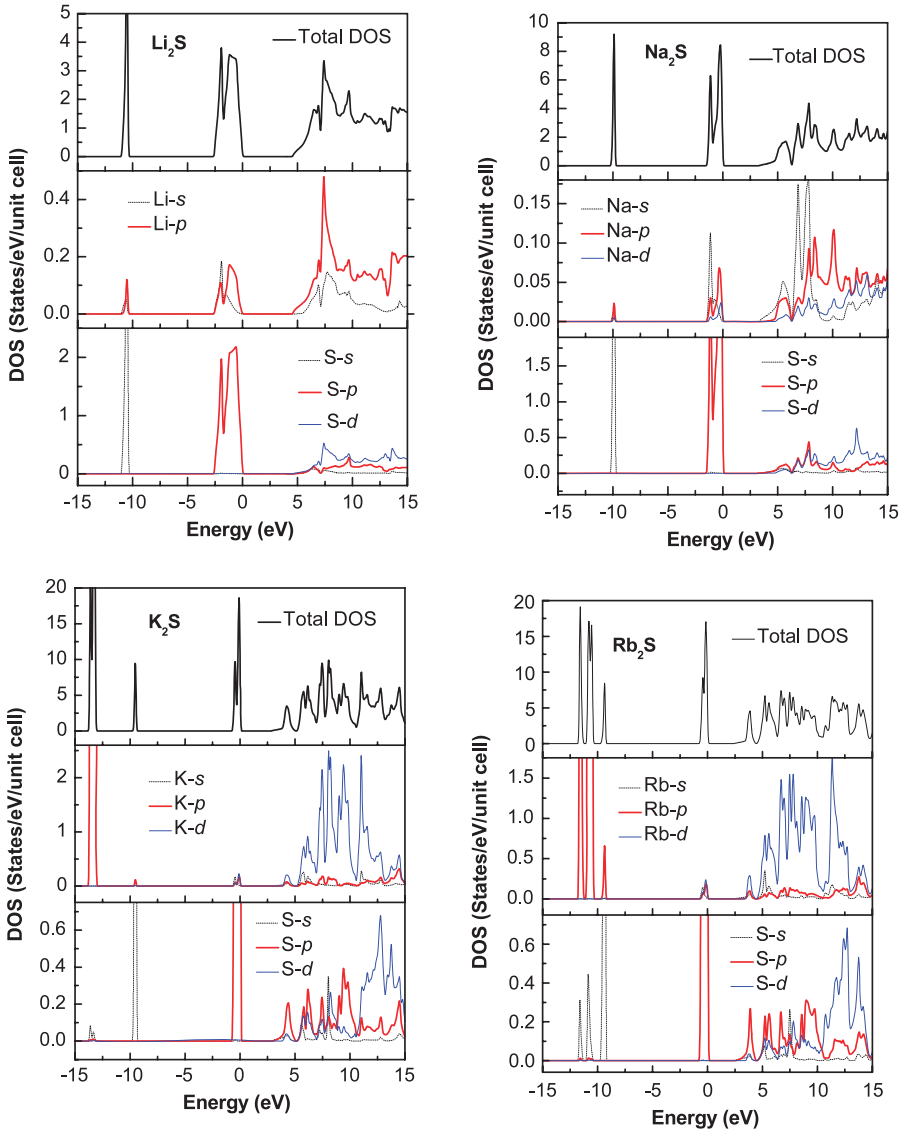

Figure 3. Total and partial densities of states for Li_2S, Na_2S, K_2S and Rb_2S compounds.

pressure coefficients, respectively. The calculated values of B and C for a direct gap (Γ–Γ and X–X) and an indirect gap (Γ–X or X–Γ) are given in table 3. The direct gaps (X–X) and (Γ–Γ) increase with increasing pressure for the four compounds studied herein. The indirect gap (Γ–X) of Li_2S decreases, while the indirect gap (X–Γ) for Na_2S, K_2S and Rb_2S increases. This is related to the bonding nature of the bottom of the conduction band, which is different between Li_2S on one hand and Na_2S, K_2S and Rb_2S on the other hand. Such behaviors are also observed in other materials [37, 38].

3.3. Optical properties

Since the alkali metal sulfides have cubic symmetry, we need to calculate only one dielectric tensor component to completely characterize the linear optical properties. In the following $\varepsilon(\omega)$ is the frequency dependent dielectric function. $\varepsilon_2(\omega)$, the imaginary part of the frequency dependent dielectric function, is given by [39]

$$\varepsilon_2(\omega) = \frac{e^2\hbar}{\pi m^2\omega^2}\sum_{v,c}\int_{\mathrm{BZ}} |M_{cv}(k)|^2\,\delta\left[\omega_{cv}(k)-\omega\right]\mathrm{d}^3k. \quad (1)$$

Table 3. Calculated first- and second-order pressure coefficients of some direct and indirect bandgaps (X–X, Γ–X and Γ–Γ) for Li_2S, Na_2S, K_2S and Rb_2S compounds in cubic antifluorite phase. $E_g(p) = E_g(0) + Bp + Cp^2$, $E_g(0)$ in eV, B in 10^{-2} eV $(\mathrm{GPa})^{-1}$, C in 10^{-4} eV $(\mathrm{GPa})^{-2}$.

	Γ–Γ		X–X		Γ–X or X–Γ	
	B	C	B	C	B	C
Li_2S						
EV-GGA	13.85	−25.4	2.90	−5.55	−1.14	−1.58
Na_2S						
EV-GGA	12.64	−25.4	4.03	−16.7	14.14	−31.7
K_2S						
EV-GGA	18.59	−45.2	3.17	−15.9	15.01	−42.9
Rb_2S						
EV-GGA	15.2	−11.1	0.82	9.92	10.73	−10.30

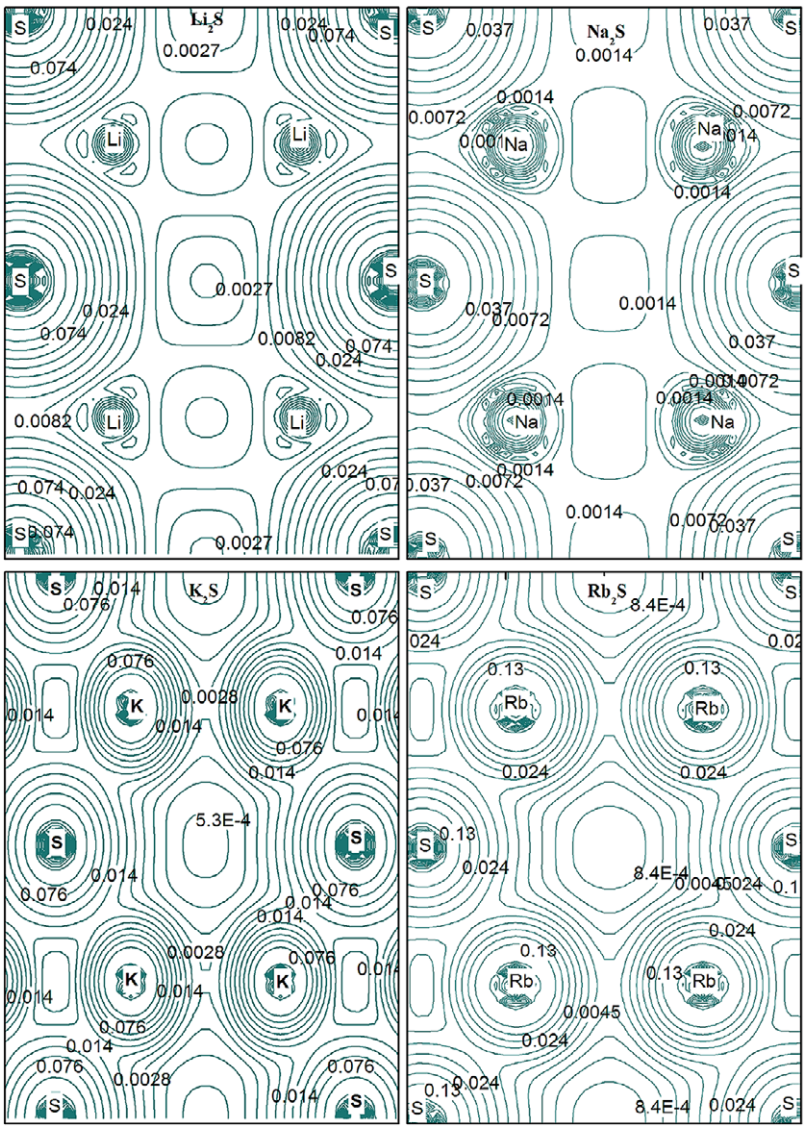

Figure 4. Total charge density contour plots in the (110) plane for K_2S, Li_2S, Na_2S, and Rb_2S compounds.

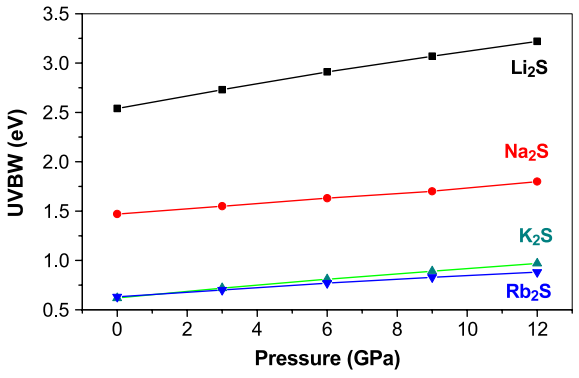

Figure 5. Pressure dependence of the upper valence bandwidth for Li_2S, Na_2S, K_2S and Rb_2S compounds.

The integral is over the first Brillouin zone. The momentum dipole elements, $M_{cv}(k) = \langle u_{ck}|\boldsymbol{\delta}\cdot\nabla|u_{vk}\rangle$, where $\boldsymbol{\delta}$ is the potential vector defining the electric field, are matrix elements for direct transitions between valence $u_{vk}(r)$ and conduction band $u_{ck}(r)$ states, and the energy $\hbar\omega_{cv}(k) = E_{ck} - E_{vk}$ is the corresponding transition energy. The real part $\varepsilon_1(\omega)$ of the frequency dependent dielectric function can be derived from the imaginary part using the Kramers–Kronig relation.

$$\varepsilon_1(\omega) = 1 + \frac{2}{\pi} P \int_0^{\infty} \frac{\omega' \varepsilon_2(\omega')}{\omega'^2 - \omega^2} \, \mathrm{d}\omega' \qquad (2)$$

where P implies the principal value of the integral. The knowledge of both real and imaginary parts of the frequency dependent dielectric function allows the calculation of important optical functions such as the refractive index $n(\omega)$:

$$n(\omega) = \left[\frac{\varepsilon_1(\omega)}{2} + \frac{\sqrt{\varepsilon_1^2(\omega) + \varepsilon_2^2(\omega)}}{2} \right]^{1/2}. \qquad (3)$$

In the calculations of the optical properties, a dense mesh of uniformly distributed $\boldsymbol{k}$-points is required. Hence, the

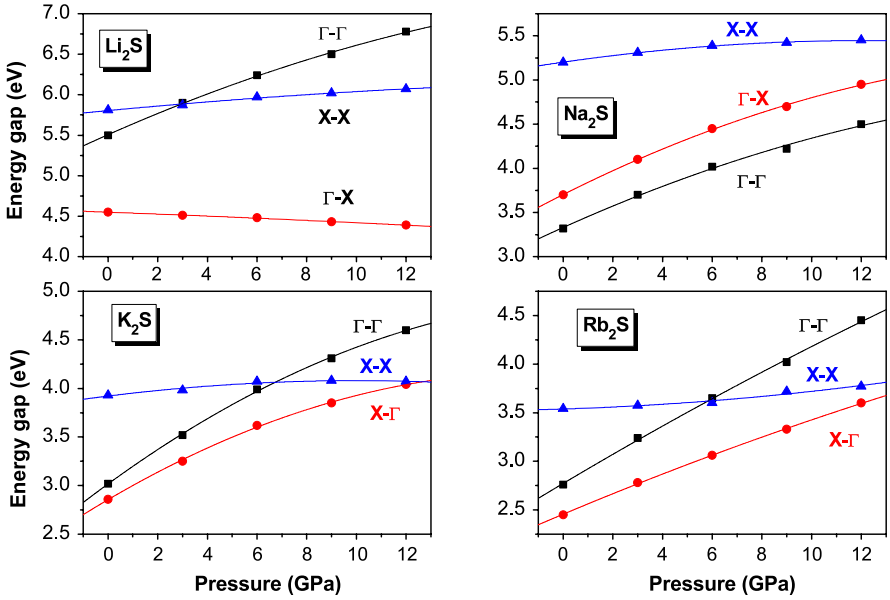

Figure 6. EV-GGA energy bandgaps versus pressure for Li_2S, Na_2S, K_2S and Rb_2S compounds.

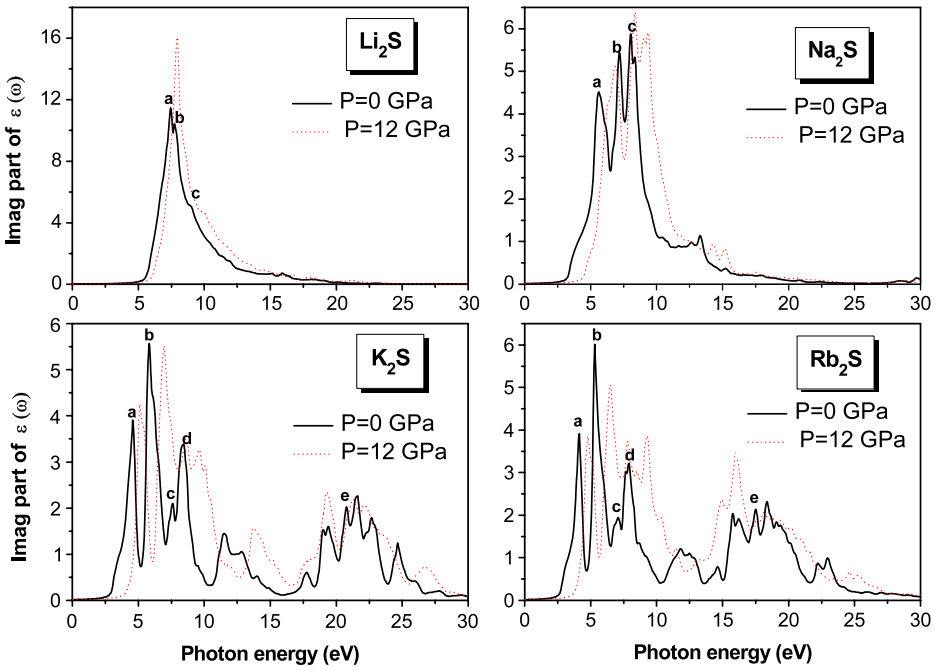

Figure 7. Calculated EV-GGA imaginary part of the dielectric function for Li_2S, Na_2S, K_2S and Rb_2S compounds at $P = 0$ GPa (solid line) and at $P = 12$ GPa (dotted line).

Brillouin zone integration was performed with 328 and 256 ***k***-points in the irreducible part of the Brillouin zone. We find very small differences between both calculations. In this work we present calculations with only 256 ***k***-points. Broadening is taken to be 0.2 eV. The EV-GGA was used to perform optical property calculations since it yields better bandgaps than LDA and GGA.

Figure 7 displays the calculated imaginary (absorptive) part of the dielectric function $\varepsilon_2(\omega)$ for Li_2S, Na_2S, K_2S and Rb_2S at ambient and at 12 GPa pressure for a radiation up to 30 eV. The real part of the dielectric function $\varepsilon_1(\omega)$ is also calculated but not presented. As can be seen, the $\varepsilon_2(\omega)$ spectrum varies greatly from Li_2S to Na_2S to K_2S (Rb_2S). This is attributed to the fact that the conduction bands are usually quite different, and the symmetries of the wavefunctions, which dictate the selection rules, are fully reflected in the matrix moment elements (MMEs). It is worthwhile to attempt to identify the interband transitions that are responsible for the structures in $\varepsilon_2(\omega)$ using our calculated band structures. To our knowledge there are no experimental or theoretical data concerning the dielectric function of Li_2S, Na_2S, K_2S and Rb_2S. Below, more detailed discussion of optical spectra is presented.

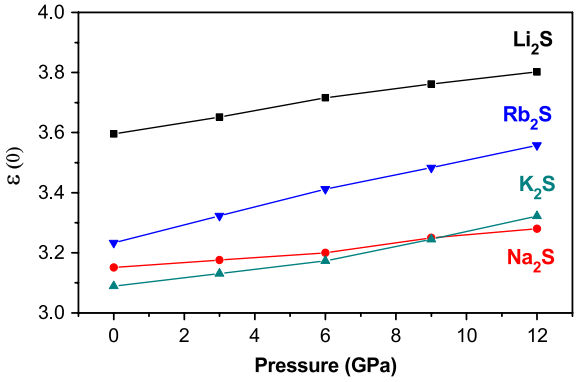

Figure 8. Pressure dependence of $\varepsilon(0)$ of Li_2S, Na_2S, K_2S and Rb_2S compounds within EV-GGA.

3.3.1. Li_2S. The dielectric function $\varepsilon_2(\omega)$ of Li_2S exhibits three structures labeled a, b and c as shown in figure 7. The threshold for direct optical transitions between the highest valence band and the lowest conduction band at the Γ-edge occurs at 5.50 eV. Beyond this structure, the $\varepsilon_2(\omega)$ curve increases rapidly. This is due to the fact that the number of points contributing to $\varepsilon_2(\omega)$ increases abruptly. Structure b, the main peak, located at 7.46 eV, is mainly due to direct transitions between the upper valence band and the second conduction band above the Fermi energy at the Γ-edge. Peak c located at 7.77 eV is related to direct transitions between the upper valence band and the conduction band along the Λ and Δ directions.

3.3.2. Na_2S. The calculated $\varepsilon_2(\omega)$ has major peaks labeled a–c in the spectrum. The threshold for direct optical transitions between the highest valence band and the lowest conduction band at the Γ-edge occurs at 3.32 eV. Structure a centered at 5.59 is due to direct transitions occurring around the L point. Structure b located at 7.20 eV corresponds to direct X–X transitions. Structure c, the main peak, located at 8.03 eV, is mainly due to direct transitions between the upper valence band and the second conduction band above the Fermi energy at the Γ-edge.

3.3.3. K_2S and Rb_2S. The K_2S and Rb_2S spectra have some features in common. The threshold for direct optical transitions between the highest valence band and the lowest conduction band at the Γ-edge for K_2S (Rb_2S) occurs at 3.02 eV (2.76 eV). Peak a located at 4.57 eV (4.09 eV) originates from direct W–W transition. The main peak, structure b, located at 5.78 eV (5.37 eV), is mainly due to direct transitions between the upper valence band and the second conduction band above the Fermi energy at the Γ-edge. The main peak is followed by three peaks, c, d and e, located at 8.4 eV, 11.45 eV and 21.5 eV (7.93 eV, 12.07 eV and 17.63 eV), respectively. Peaks c and d are related to direct transitions between the upper valence band and the conduction band along the Λ and Δ directions. The third peak originates from direct transitions between the valence band situated at about −10 eV and the conduction band along the Λ, Δ and W–L directions.

Table 4. Calculated dielectric constant $\varepsilon(0)$, pressure and volume coefficients of refractive index for Li_2S, Na_2S, K_2S and Rb_2S compounds in cubic antifluorite phase.

	$\varepsilon(0)$	$\frac{1}{n_0}\frac{dn}{dp}(10^{-4}\ \mathrm{GPa}^{-1})$	$\frac{V_0}{n_0}\frac{dn}{dV}$
Li_2S	3.60	23.83	−0.15
Na_2S	3.15	17.91	−0.09
K_2S	3.09	30.72	−0.12
Rb_2S	3.23	40.7	−0.16

It is obvious that the sulfur p states and metal s, p and d states play the major role in these optical transitions as initial and final states, respectively. Spin–orbit coupling does not have any significant effect on the results. This is what we expected, since the spin–orbit coupling changes the eigenvalues only by around 0.1 eV, which does not have a significant influence on the calculations of the optical properties. This has also been found in previous FP-LAPW and FP-LMTO calculations for WSe_2 and SrX [40, 41].

When we compress these materials, the positions of all critical points cited above are shifted towards higher energies. The reason lies in the enhancement of different gaps under pressure. Although the positions of all peaks are shifted under pressure, they still have the same type as those at zero pressure, with increasing/decreasing intensity of the main and secondary peaks.

At high frequencies the zero crossing of $\varepsilon_1(\omega)$, which corresponds to the location of the screened plasma frequency, is located at 17.37, 14.32, 25.45 and 23.76 eV for Li_2S, Na_2S, K_2S and Rb_2S, respectively. The static dielectric constant $\varepsilon_1(0)$ is given by the low energy limit of $\varepsilon_1(\omega)$. It is necessary to emphasize that we do not include phonon contributions to the dielectric screening, and $\varepsilon_1(0)$ corresponds to the static optical dielectric constant ε_∞. The calculated optical dielectric constants ε_∞ are listed in table 4. Figure 8 shows the pressure dependence of the dielectric constant $\varepsilon(0)$ for Li_2S, Na_2S, K_2S and Rb_2S compounds within the EV-GGA formalism. As can be seen, the increase of the static dielectric constant (static refractive index) with pressure is practically linear in all the compounds. The pressure derivatives of the refractive index n of these compounds are determined by a linear fit. The calculated pressure and volume coefficients of refractive index are also listed in table 4. To our knowledge, there are no experimental or theoretical results for the optical properties available for these compounds, so the present results can be considered as a predictive study, hopping that the present work will stimulate some other works on these materials.

4. Conclusions

We have performed a detailed investigation on the structural, electronic and optical properties of Li_2S, Na_2S, K_2S and Rb_2S compounds with and without applied pressure using the first-principles FP-APW + lo method within LDA, GGA and EV-GGA. The most relevant conclusions are summarized as follows. (i) The calculated ground-state properties such as lattice parameter, bulk modulus and its pressure derivative agree quite well with the available experimental and theoretical

results. (ii) The calculated band structures show also that the Li_2S, K_2S and Rb_2S are indirect bandgap materials, whereas Na_2S is a direct gap material. (iii) Results obtained for band structure using EV-GGA are larger than those within LDA and GGA. (iv). The bonding character has been discussed in terms of the electron charge density and it shows a strong localization around the anion. (v) The critical point structure of the frequency dependent complex dielectric function was investigated and analyzed to identify the optical transitions. (vi) The spin–orbit coupling does not have any significant effect on the electronic and optical properties. (vii) To the best of our knowledge, there are no earlier studies on the effect of pressure on the electronic structure and imaginary part of the dielectric constant; we feel that our calculations can be used to cover the lack of data for these compounds.

Acknowledgments

For the author Ali Hussain Reshak this work was supported from the institutional research project of the Institute of Physical Biology, UFB (No MSM6007665808), and the Institute of System Biology and Ecology, ASCR (No AVOZ60870520).

References

[1] Shunk F A (ed) 1969 *Constitution of Binary Alloys* (New York: McGraw-Hill) 2nd Suppl.
[2] Yao W and Martin S W 2008 *Solid State Ion.* **178** 1777
[3] Takada K, Inada T, Kaiyama A, Kouguchi M, Sasaki H, Kondo S, Michiue Y, Nakano S, Tabuchi M and Watanabi M 2004 *Solid State Ion.* **172** 25
[4] Zhou Y, Wu C, Zhang H, Wu X and Fu Z 2007 *Electrochim. Acta* **52** 3130
[5] Wen Z, Huang S, Yang X and Lin B 2008 *Solid State Ion.* **179** 1800
[6] Minami T, Hayashi A and Tatsumisago M 2000 *Solid State Ion.* **136** 1015
[7] Bührer W, Altorfer F, Mesot J, Bill H, Carron P and Smith H J 1991 *J. Phys.: Condens. Matter* **3** 1055
[8] Bührer W and Bill H 1977 *Helv. Phys. Acta* **50** 431
[9] Grzechnik A, Vegas A, Syassen K, Loa L, Hanfland M and Jansen M 2000 *Solid. State Chem.* **154** 603
[10] Vegas A, Grzechnik A, Syassen K, Loa L, Hanfland M and Jansen M 2001 *Acta Crystallogr.* B **57** 151
[11] Vegas A, Grzechnik A, Hanfland M, Muhle C and Jansen M 2002 *Solid State Sci.* **4** 1077
[12] Lichanot A, Aprà E and Dovesi R 1993 *Phys. Status Solidi* b **177** 157
[13] Bührer W and Bill H 1980 *J. Phys. C: Solid State Phys.* **13** 5495
[14] Schön J C, Cancarevic Z and Jansen M 2004 *J. Chem. Phys.* **121** 2289
[15] Zhuravlev Y N, Kosobutskii A B and Poplavnoi A S 2005 *Russ. Phys. J.* **48** 138
[16] Azavant P, Lichanot A and Rérat M 1994 *Acta Crystallogr.* B **50** 279
[17] Eithiraj R D, Jaiganesh G, Kalpana G and Rajagopalan M 2007 *Phys. Status Solidi* b **244** 1337
[18] Gao S 2003 *Comput. Phys. Commun.* **153** 190
[19] Schwarz K 2003 *J. Solid State Chem.* **176** 319
[20] Madsen G K H, Blaha P, Schwarz K, Sjöstedt E and Nordström L 2001 *Phys. Rev.* B **64** 195134
[21] Schwarz K, Blaha P and Madsen G K H 2002 *Comput. Phys. Commun.* **147** 71
[22] Blaha P, Schwarz K, Madsen G K H, Kvasnicka D and Luitz J 2001 WIEN2k, An augmented plane wave plus local orbitals program for calculating crystal properties, Vienna University of Technology, Austria
[23] Perdew J P and Zunger A 1981 *Phys. Rev.* B **23** 5048
[24] Perdew J P, Burke S and Ernzerhof M 1996 *Phys. Rev. Lett.* **77** 3865
[25] Engel E and Vosko S H 1993 *Phys. Rev.* B **47** 13164
[26] Monkhorst H J and Pack J D 1976 *Phys. Rev.* B **13** 5188
[27] Birch F 1978 *J. Geophys. Res.* **83** 1257
[28] Zintl E, Harder A and Dauth B 1934 *Z. Elektrochem.* **40** 588
[29] Onida G, Reining L and Rubio A 2002 *Rev. Mod. Phys.* **74** 601
[30] Fahy S, Chang K J, Louis S G and Cohen M L 1989 *Phys. Rev.* B **35** 7840
[31] Dufek P, Blaha P and Schwarz K 1994 *Phys. Rev.* B **50** 7279
[32] Bouhemadou A, Khenata R, Zegrar F, Sahnoun M, Baltache H and Reshak A H 2006 *Comput. Mater. Sci.* **38** 263
[33] Wu X, Qin S and Wu Z 2007 *Phys. Rev.* B **73** 134103
[34] Hoffman R 1988 *Rev. Mod. Phys.* **60** 801
[35] Gellatt C D Jr, Williams A R and Moruzzi V L 1983 *Phys. Rev.* B **27** 2005
[36] Lin G Q, Gong H and Wu P 2005 *Phys. Rev.* B **71** 85203
[37] Kalpana G, Palanivel B and Rajagopalan M 1995 *Phys. Rev.* B **52** 4
Kalpana G, Palanivel B and Rajagopalan M 1994 *Phys. Rev.* B **50** 12318
[38] Kanchana V, Vaitheeswaran G and Rajagopalan M 2003 *Physica* B **328** 283
[39] Ambrosch-Draxl C and Sofo J O 2006 *Comput. Phys. Commun.* **175** 1
[40] Sharma S, Ambrosch-Draxl C, Khan M A, Blaha P and Auluck S 1999 *Phys. Rev.* B **60** 8610
[41] Dadsetani M and Pourghazi A 2006 *Phys. Rev.* B **73** 195102